Nanoscale

COMMUNICATION

View Article Online
View Journal | View Issue

Published on 05 August 2014. Downloaded by Michigan State University on 23/01/2016 07:14:54.

Cite this: *Nanoscale*, 2014, **6**, 11078

Received 23rd May 2014
Accepted 25th July 2014

DOI: 10.1039/c4nr02817a

www.rsc.org/nanoscale

Self-assembly of hybridized ligands on gold nanodots: tunable photoluminescence and sensing of nitrite†

Wei-Yu Chen,[a] Chih-Ching Huang,*[bcd] Li-Yi Chen[a] and Huan-Tsung Chang*[a]

Highly photoluminescent gold nanodots (Au NDs) *via* etching and co-deposition of hybridized ligands [11-mercaptoundecanol (11-MU) and its complexes with amphiphilic ligands] on gold nanoparticles (~3 nm) have been prepared and employed for the detection of nitrite based on the analyte-induced photoluminescence quenching.

Quantum-size gold (Au) nanoclusters (NCs) and nanodots (NDs) have become interesting sensing materials because of their molecule-like photoluminescence (PL) properties, such as large Stokes shift, long lifetime, and biocompatibility.[1] For example, photoluminescent thiolate-protected Au NDs, each composed of a crystalline Au core and an Au–thiolate complex shell, have been used for detecting various analytes such as Hg^{2+} ions.[2] Photoluminescent alkanethiol-protected Au NDs are commonly prepared by etching small sizes of Au nanoparticles (NPs) (*ca.* 3.0 nm) under alkaline conditions using alkanethiols such as 2-mercaptoethanol, 6-mercaptohexanol, and 11-mercaptoundecanoic acid (11-MUA).[3] The sizes of the photoluminescent Au NDs (2.0 nm; ca. Au_{200}) represent a missing link between Au NCs (<Au_{100}) and large Au NPs (Au NPs; >3 nm).[1,4] Unlike Au NCs, the PL properties of Au NDs are related not only directly to their core sizes but also to electronic transitions of surface Au(I) coupling to the ligand–metal charge transfer transition.[3,5–7] As a result, by varying alkyl chain lengths and functional groups of alkanethiols, different PL colors of Au NDs can be prepared.[3] In addition to PL properties, the capping ligands alter the chemical reactivity and stability of Au NDs.[8]

Formation of a self-assembled bilayer on the surface of Au NDs has been demonstrated for improved dispersibility, PL intensity, and photostability.[9] In addition, desired functionality can be introduced onto the surface of each Au ND *via* self-assembly of biofunctional ligands with surface 11-MUA molecules through hydrophobic patches and/or electrostatic interactions. For example, 11-MUA-capped Au NDs (11-MUA–Au NDs) self-assembled with phospholipids have greater PL quantum yields and stabilities relative to 11-MUA–Au NDs. By taking advantage of the high affinity and catalytic activity of phospholipase C for phospholipids, phospholipid functional Au NDs have been used to detect phospholipase C, based on analyte-induced PL quenching.[9] Since the chemical and optical properties of bilayer-protected Au NDs can be varied by changing the functional ligands, it is expected that different functional Au NDs protected with bilayers of hybridized ligands can be prepared for catalysis, sensing, molecular targeting, and cell imaging.[1,10,11]

Here, we report a comprehensive study of the effects of amphiphilic ligands (ALs), including fatty acids (FAs) and quaternary ammonium surfactants (QASs), on the synthesis of thiolate-protected Au NDs through core etching of Au NPs (a top-down approach). Although we have reported that the deposition of alkanethiols (RSH) onto the surfaces of Au NPs (~3.0 nm) results in the formation of photoluminescent RS–Au NDs,[3] great effort in this study is made to prepare hybrid-ligand co-deposited Au NDs for improving Au NDs' quantum yield (QY), stability and water solubility. Each 11-mercaptoundecanol-capped-Au ND (11-MU–Au ND) was decorated with an AL shell through nonspecific hydrophobic interactions between the alkyl chains of the ALs and the 11-MU molecules on Au ND surfaces. The effects of alkyl chain length and charge of the ALs on optical properties of AL/11-MU–Au NDs were investigated. Self-assembly of AL/11-MU bilayers not only improves the dispersion of Au NDs in aqueous solution but also affects their PL properties, including quantum yields (QYs), Stokes shifts,

[a]*Department of Chemistry, National Taiwan University, 1, Section 4, Roosevelt Road, Taipei 10617, Taiwan. E-mail: changht@ntu.edu.tw; Fax: +886-2-33661171; Tel: +886-2-33661171*

[b]*Institute of Bioscience and Biotechnology, National Taiwan Ocean University, 2, Pei-Ning Road, Keelung, 20224, Taiwan. E-mail: huanging@ntou.edu.tw; Fax: +886-2-24622034; Tel: +886-2-24622192 extn 5517*

[c]*Center of Excellence for Marine Bioenvironment and Biotechnology (CMBB), National Taiwan Ocean University, 2, Pei-Ning Road, Keelung, 20224, Taiwan*

[d]*School of Pharmacy, College of Pharmacy, Kaohsiung Medical University, 100, Shih-Chuan 1st Road, Kaohsiung 80708, Taiwan*

† Electronic supplementary information (ESI) available: Experimental section and Fig. S1–S9. See DOI: 10.1039/c4nr02817a

This journal is © The Royal Society of Chemistry 2014

Published on 05 August 2014. Downloaded by Michigan State University on 23/01/2016 07:14:54.

and emission lifetimes. Tetradecanoic acid (TA)/11-MU co-capped Au NDs (TA/11-MU–Au NDs) were used to detect nitrite (NO_2^-) ions, which have proved to be a threat to human health.[12] Highly NO_2^--induced PL quenching of Au NDs was observed mainly through oxidation of Au(0) atoms to Au(I) in the cores of Au NDs. The practicality of a TA/11-MU–Au ND probe was validated by analyses of tap water, lake water, and seawater.

In this study, Au NPs with a mean size of ~3 nm were synthesized through reduction of Au^{3+} mediated by tetrakis(hydroxymethyl)phosphonium chloride (THPC) that acted as both a reducing and capping agent.[13] Under alkaline conditions, an 11-MU solution or a solution of 11-MU and AL was used to etch the as-prepared Au NPs. Deposition of 11-MU or co-deposition of AL/11-MU onto the surfaces of the as-prepared Au NPs allows preparation of 11-MU–Au NDs or AL/11-MU–Au NDs (Scheme 1b). Two ALs, TA and myristyltrimethylammonium bromide (MTAB), were first employed in the synthesis of AL/11-MU–Au NDs. Fig. 1 displays the absorption and PL spectra of 11-MU–Au NDs, TA/11-MU–Au NDs, and MTAB/11-MU–Au NDs. The three TEM images (Fig. S1, ESI†) reveal that the sizes of the 11-MU–Au NDs, TA/11-MU–Au NDs, and MTAB/11-MU–Au NDs were 2.49 ± 0.30 nm, 2.03 ± 0.28 nm, and 1.99 ± 0.33 nm, respectively, based on 100 counts for each. The three high-resolution TEM (HRTEM) images displayed in the insets of Fig. S1† reveal that the lattice fringes of all as-prepared Au NDs were consistent with metallic gold having a discerned lattice spacing of 2.38 Å, which corresponds to the *d*-spacing of the (111) crystal plane of fcc Au.[3] Unlike the surface plasmon resonance (SPR) absorption of large Au NPs (>3 nm), small sized Au NDs and Au NCs (<2 nm) lack an apparent SPR band. Briefly,

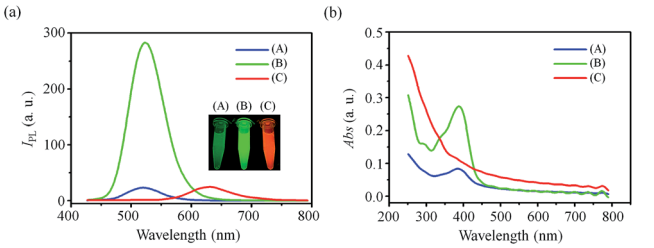

Fig. 1 (a) PL and (b) UV-vis absorption spectra of (A) 11-MU–Au NDs, (B) TA/11-MU–Au NDs, and (C) MTAB/11-MU–Au NDs in 10 mM sodium phosphate solutions (pH 7.0). The 11-MU–Au NDs, TA/11-MU–Au NDs, and MTAB/11-MU–Au NDs were obtained from the reactions of THPC–Au NPs (3 nm) with 11-MU (1.0 mM), 11-MU (1.0 mM)/TA (2.5 mM), and 11-MU (1.0 mM)/MTAB (0.25 mM) in 20 mM sodium tetraborate (pH 9.2) at ambient temperature for 48 h, respectively. Inset in (a): photogram of the three corresponding Au ND solutions upon excitation under a hand-held UV lamp (365 nm). Absorbance (Abs) and PL intensities (I_{PL}) are plotted in arbitrary units (a. u.). Excitation wavelengths in (a) for 11-MU–Au NDs and TA/11-MU–Au NDs were set at 390 nm and that for MTAB/11-MU–Au NDs was at 275 nm.

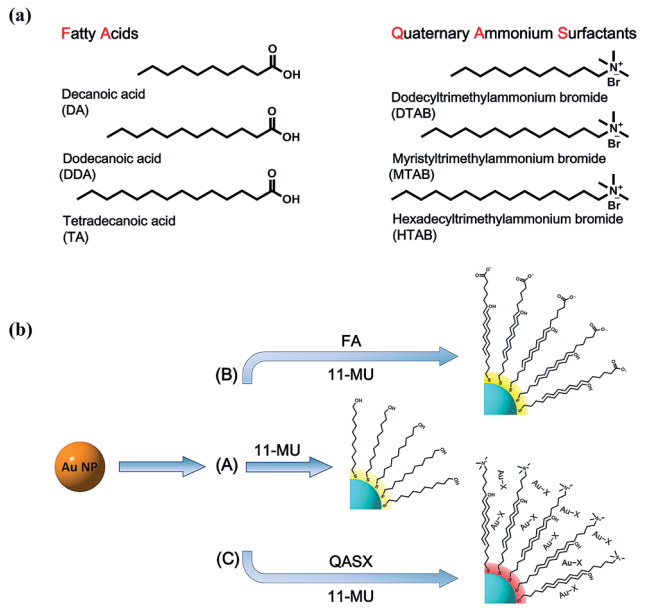

Scheme 1 (a) Chemical structures of the amphiphilic ligands used for the synthesis of photoluminescent Au NDs. (b) Schematic representation of the synthesis of photoluminescent (A) 11-MU–Au NDs, (B) FA/11-MU–Au NDs, and (C) QAS/11-MU–Au NDs. Au–X complexes were formed between the Au^{3+} ions and X^- (Cl^-, Br^- and phosphine-containing ions).

we inferred that the absorption of 11-MU–Au NDs and TA/11-MU–Au NDs at 390 nm with absorption coefficient (ε) values of *ca.* $8.4 \times 10^5\ M^{-1}\ cm^{-1}$ and $2.7 \times 10^6\ M^{-1}\ cm^{-1}$ originated from ligand-to-metal ND charge transfer (LMNCT; S → Au) mixed with ligand-to-metal–metal charge transfer (LMMCT; S → Au···Au) on the particle surface.[8a] The formation of TA/11-MU complexes through hydrophobic interactions increased the solubility of 11-MU and made it easier to access the surfaces of Au cores and etch Au atoms. As a result, TA/11-MU–Au NDs exhibited higher absorbance at 390 nm (Fig. 1b, curve B) and smaller particle sizes (2.49 nm *vs.* 2.03 nm). The zeta potentials of 11-MU–Au NDs and TA/11-MU–Au NDs were −14.55 ± 0.36 mV ($n = 5$) and −19.45 ± 0.55 mV ($n = 5$), respectively. The slight increase in the zeta potential in the presence of TA ligands suggests that TA anions were bound to the surfaces of the 11-MU–Au NDs. We further determined the surface components of purified TA/11-MU–Au NDs by laser desorption/ionization time-of-flight mass spectrometry. The peak at m/z 227.171 corresponds to $[TA–H]^-$, confirming the existence of TA molecules on the Au ND surfaces (Fig. S2a, ESI†). In comparison with the 11-MU–Au NDs [$\tau_1 = 92.1$ ns (43.17%) and $\tau_2 = 4.80$ ns (56.83%)], the TA/11-MU–Au NDs had longer lifetimes [$\tau_1 = 115.48$ ns (54.11%) and $\tau_2 = 5.63$ ns (45.89%)] (data not shown). The TA/11-MU–Au NDs had a densely packed ligand shell on each core, stronger PL, and smaller size. The large Stokes shift (>130 nm) and long lifetime suggest that the emission from TA/11-MU–Au NDs is mainly from a low-lying triplet state (phosphorescence) that is populated *via* intersystem crossing from the lowest singlet state.[3,5,6] Thus, we suspect a high degree of polynuclear Au(I)–thiolate complexes formed in the shell of each core in the TA/11-MU–Au NDs and the PL of Au NDs mainly originated from Au ND/polynuclear Au(I)–thiolate (core/shell) complexes.

Relative to 11-MU–Au NDs, the TA/11-MU–Au NDs had a higher QY [2.57% *vs.* 1.31%], which was determined by comparing with quinine (QY = 53%). The densely packed ligand

Published on 05 August 2014. Downloaded by Michigan State University on 23/01/2016 07:14:54.

shell (higher order of Au(I)–thiolate/FAs complex) formed on Au ND surfaces strengthened aurophilic Au(I)–Au(I) interactions, leading to the stronger PL intensity.[3] In addition, it is more difficult for quenchers such as O_2 to access the surfaces of Au cores.[9] We also found that the PL intensity of FA/11-MU–Au NDs was highly dependent on the surface density and chain length of FAs (Fig. S3, ESI†). The higher concentration and longer chain length of FAs result in stronger hydrophobic interactions (dispersion force) between 11-MU and FAs, thereby resulting in a more stable packing shell on the surface of each Au ND.[14] Our results suggest that a more dense ligand shell of FA/11-MU on the surface of each Au ND can minimize its PL quenching as a result of fewer collisions with quenchers (*e.g.*, oxygen molecules, solvent molecules, hydroxyl ions, halide ions) in solution. Fewer collisions also minimize the number of internal non-radiative relaxation pathways (*e.g.*, restrain on intramolecular vibrations and rotations).[15] We could not exclude the possibility that charged dense-ligand shells on Au ND surfaces prevent interparticle collision-induced PL quenching.[16]

When positively charged MTAB ions were present on the surfaces of Au NDs *via* strong hydrophobic interactions with 11-MU units, anions such as Cl^-, Br^-, and ions containing phosphine, were attracted to Au ND surfaces through electrostatic interactions (Scheme 1b, route c).[17] Therefore, a dense mixture shell of Au(I)–11-MU/MTAB and Au(I)–X (X: halide ions or phosphine-containing ions) formed on the surface of each Au ND, leading to a broader absorption band.[18] The positive zeta potential of MTAB/11-MU–Au NDs [2.35 ± 0.93 mV ($n = 5$)] and observation of a peak of $[MTAB–Br]^+$ at m/z 256.298 (Fig. S2b, ESI†) reveal that myristyltrimethylammonium cations did indeed self-assemble on the surfaces of the 11-MU–Au NDs. Owing to their low zeta potential, the MTAB/11-MU–Au NDs aggregated (Fig. S1c, ESI†) and, after two days, some particles readily settled in the solution. The absorption and PL spectra of MTAB/11-MU–Au NDs (curve C in Fig. 1) show a strong resemblance to that of the oligomeric Au(I)–thiolate complexes: the absorption band onset at ~400 nm and of the emission band at 630 nm are both broad. The result suggests that the formation of oligomeric Au(I)–thiolate complexes on the surfaces of Au NDs is responsible for the enhanced PL intensity. In addition, the PL of MTAB/11-MU–Au NDs also likely arises from the decay of excited electrons from higher energy states in the sp-band of the surface Au atoms/ions to hybrid electronic states (p orbital of S or X; X: halide ions or phosphine-containing ions) of surface Au–S and/or Au–X.[4b,19] Therefore, we suspect that the PL of MTAB/11-MU–Au NDs is from the Au cores and dense polynuclear Au(I)–11-MU/MTAB and Au(I)–X complexes on the Au ND surfaces.

The QY of MTAB/11-MU–Au NDs was determined to be 37% through comparison with $Cs_3[Eu(dpa)_3]$ (QY = 24%; $\lambda_{ex} = 279$ nm; $\lambda_{em} = 590$–700 nm). The QY of the MTAB/11-MU–Au NDs is comparable with those of the best currently available water-soluble alkanethiol-protected metallic NDs and NCs.[20] The much shorter PL lifetime of MTAB/11-MU–Au NDs [$\tau_1 = 70.44$ ns (31.50%) and $\tau_2 = 3.46$ ns (68.50%)] suggests that large numbers of Au(I)–X complexes (weak donating electron from X^-) were present on Au ND surfaces.[17] The existence of Au(I)–thiolate and Au(I)–X complexes in the photoluminescent Au NDs was confirmed by X-ray photoelectron spectroscopy (XPS) analyses (Fig. S4, ESI†). The Au $4f_{7/2}$ spectrum of the photoluminescent Au NDs was deconvoluted into Au(I) and Au(0) components with binding energies (BEs) of 85.0 and 83.6 eV, respectively. Compared with 11-MU–Au NDs (62.0%) and TA/11-MU–Au NDs (63.2%), the slightly higher Au(I) content in MTAB/11-MU–Au NDs (69%) is likely due to the dense polynuclear Au(I)–11-MU/MTAB and Au(I)–X complexes on Au ND surfaces.[18] These highly dense polynuclear Au(I)–11-MU/MTAB and Au(I)–X complexes also contributed to the higher QY. We also found that the PL properties of 11-MU–Au NDs are more closely related to the surface density of cationic QASs rather than to its chain length (Fig. S5, ESI†). Upon increasing the concentration of QASs, the PL intensity of QAS/11-MUA–Au NDs at 630 nm increased, reaching a plateau at 0.25 mM for MTAB and CTAB and reaching 0.50 mM for DTAB. When the concentrations of QASs were increased from 0 to 0.25 or 0.50 mM, more Au(I)–11-MU/QAS and Au(I)–X were co-deposited on the Au NDs, leading to increased PL intensity at 630 nm. At higher concentrations of QAS (>0.25 or 0.5 mM), the major species in the shells of Au NDs were polynuclear Au(I)–11-MU/QAS complexes. However, the PL intensity at 520 nm decreased upon increasing the QAS concentration from 0 to 0.5 mM or 1.0 mM. On further increasing the QAS concentration to above 0.5 mM or 1.0 mM, the PL at 520 nm increased, mainly due to the complicated cooperative and/or competitive deposition of Au(I)–11-MU/MTAB and Au(I)–X on Au ND surfaces. The highly ordered, layered supramolecular structures of Au(I)–11-MU/QAS in the shells of Au NDs are responsible for PL at 520 nm.

Next, we tested the practicality of using unpurified AL/11-MU–Au NDs for sensing NO_2^- ions. Excessive concentrations of NO_2^- in oceans, rivers, and drinking water pose a serious threat to human health and aquatic organisms.[12] We first examined the effects of NO_2^- ions on the PL of the 11-MU–Au NDs, TA/11-MU–Au NDs, and MTAB/11-MU–Au NDs. We considered the relative PL intensities $[(I^0_{PL} - I_{PL})/I^0_{PL}]$ at 520 nm (11-MU–Au NDs and TA/11-MU–Au NDs) and 630 nm (MTAB/11-MU–Au NDs), where I^0_{PL} and I_{PL} are the PL intensities of the Au NDs (50 nM) in 10 mM sodium phosphate solution (pH 3.0), in the absence and presence of NO_2^- ions (1.0 μM), respectively. We found that NO_2^- ions induced a greater quenching efficiency $[(I^0_{PL} - I_{PL})/I^0_{PL}]$ to TA/11-MU–Au NDs (45.3%) than to 11-MU–Au NDs (7.72%) and MTAB/11-MU–Au NDs (1.21%). This result is mainly due to strong electrostatic interactions of TA/11-MU–Au NDs with the intermediate (nitrosyl cations; NO^+) of NO_2^- ions. To understand NO_2^--induced PL quenching of Au NDs, we performed zeta potential, light scattering, and XPS measurements. The slight changes in the zeta potentials (-19.45 ± 0.55 mV *vs.* -18.32 ± 0.21 mV) and static light scattering (174.7 ± 19.7 kcps *vs.* 193.9 ± 20.4 kcps) of TA/11-MU–Au NDs in the absence and presence of 100 μM NO_2^- rule out NO_2^--induced PL quenching due to changes in particle sizes or aggregation. The BE values for Au $4f_{7/2}$ electrons in TA/11-MU–Au NDs (100 nM) in the absence and presence of NO_2^- ions were 84.2 eV and 85.3 eV (Fig. S4d, ESI†), respectively, revealing that NO_2^- induced an increase in the oxidation of core Au(0) of Au NDs to

 This journal is © The Royal Society of Chemistry 2014

Published on 05 August 2014. Downloaded by Michigan State University on 23/01/2016 07:14:54.

Au(I).[21] Because PL intensity was dramatically influenced by the polynuclear Au(I)–thiolate units on the surface, presumably, the NO_2^--induced PL quenching was mainly caused by oxidation of Au(0) atoms to Au(I) in the core of Au NDs mediated by the NO_2^- ions through electron transfer between the NO_2^- ions and Au(0) units under acidic conditions.[21b,c] The oxidation of core Au(0) of Au NDs to Au(I) induced loss of polynuclear Au(I)–thiolate in the shell; as a result, its PL intensity was quenched. We also noted the PL of Au NDs not only related to the surface Au(I)–thiolate complex but also the oxidation state of the Au core.[4b,18,19] Relative to the infrared-emitting Au NCs having only few Au atoms, the energy levels of the hybrid states (*p*-orbitals of sulfur (S) with the 6*sp* orbitals of surface Au atoms/ions) of Au NDs are probably lower than the states in the *d*-band of the surface Au atom/ions.[4b,18,19] As a result, our photoluminescent Au NDs emitting at ~520 nm possibly arise from *sp* to *d*-band transitions. Therefore, we suggest that the NO_2^- induced PL quenching is mainly due to a decrease in the PL of the Au core. We observed serious PL quenching of TA/11-MU–Au NDs in the presence of NO_2^-, but only very slight changes were observed in the absorption at 390 nm (Fig. S6, ESI†). This result further supports that NO_2^- only caused the oxidation of core Au(0) to Au(I) rather than induced changes in the structure of polynuclear Au(I)–thiolate complexes on Au ND surfaces.

The NO_2^--induced PL quenching of TA/11-MU–Au NDs was well fitted with the Stern–Volmer equation ($I_{PL}^0/I_{PL} = 1 + K_{sv}[NO_2^-]$), where I_{PL}^0 and I_{PL} are the PL intensities at 520 nm in the absence and presence of NO_2^-, respectively; K_{sv} is the Stern–Volmer quenching constant; and $[NO_2^-]$ is the concentration of NO_2^-. We estimated K_{sv} to be $4.8 \times 10^5\ M^{-1}$ based on the Stern–Volmer plot (Fig. S7a, ESI†). Fig. S7b (ESI†) reveals that the NO_2^--induced PL quenching reaction reached completion within 120 s. Since the PL intensity of TA/11-MU–Au NDs also depends on temperature, the temperature effect on the NO_2^--induced PL quenching was not studied. Under constant conditions, the NO_2^--induced PL quenching follows the trend of the Stern–Volmer equation. For simple and fast analysis of NO_2^- by using the TA/11-MU–Au ND probe, the quenching reaction was performed at room temperature for 5 min.

Over the pH range from 3.0 to 11.0, we found that pH 3.0 provided the greatest PL quenching of TA/11-MU–Au NDs (Fig. S8, ESI†). In an acid medium, NO_2^- anions reacted with H^+ ions to form nitrous acid, which further reacted with H^+ ions to form NO^+ cations ($NO_2^- + 2H^+ \leftrightarrow NO^+ + H_2O$).[22] Electron deficient NO^+ ions easily oxidize TA/11-MU–Au ND through an electron transfer process.[21c] In addition, the nitrite ion is a strong oxidizer ($2HNO_2 + 4H^+ + 4e^- \leftrightarrow N_2O + 3H_2O$; $E^0 = 1.29$ V) under acidic conditions;[23] therefore, it could directly induce the oxidation of Au NDs. Comparison with Au(I) ($Au(I) + e^- \rightarrow Au(0)$; $E^0 = 1.68$ V), Au(I)–SR exhibits a lower standard reduction potential ($Au(I)–SR + e^- \rightarrow Au(0) + RS^-$; $E^0 \sim 0.6$–1.0 V). Therefore, nitrite ($2HNO_2 + 4H^+ + 4e^- \rightarrow N_2O + 3H_2O$; $E^0 = 1.29$ V) or its intermediate ($NO^+ + 4e^- \rightarrow NO$; $E^0 = 1.45$ V) could oxidize TA/11-MU–Au NDs. As a result of electrostatic repulsions, it is more difficult for NO^+ ions to access surfaces of MTAB/11-MU–Au NDs than of TA/11-MU–Au NDs. Therefore, MTAB/11-MU–Au NDs are not sensitive for NO_2^- ions. Moreover, relative to TA/11-MU–Au NDs, 11-MU–Au NDs were less stable at pH 3.0, and thus they are not useful for detecting NO_2^- ions.

As shown in Fig. 2a, the specificity of TA/11-MU–Au NDs for detecting NO_2^- ions in 10 mM sodium phosphate solution (pH 3.0) was excellent [by at least 100-fold over other tested anions: CO_3^{2-}, SO_3^{2-}, SO_4^{2-}, $S_2O_8^{2-}$, acetate (Ac^-), citrate, EDTA, CN^-, SCN^-, NO_3^-, F^-, Cl^-, Br^-, I^-, ClO_4^-, BrO_3^-, IO_3^-, IO_4^-, S^{2-}, and PO_4^{3-}]. I_{PL}^0 and I_{PL} represent PL intensities of TA/11-MU–Au NDs in the absence and presence of anions, respectively. Under acidic conditions, protonation of S^{2-} (HS^- or H_2S) and CN^- (HCN) occurred, minimizing their reactions with Au NDs through the formation of strong Au–S and Au–CN bonds. We also noted that nitrite and its intermediate possess stronger oxidation ability for the oxidation of Au NDs than that of NO_3^- ($NO_3^- + 4H^+ + 3e^- \rightarrow NO + H_2O$; $E^0 = 0.96$ V) and IO_3^- ($IO_3^- + 5H^+ + 4e^- \rightarrow HIO + 2H_2O$; $E^0 = 1.13$ V) ions. In addition, the intermediate (NO^+) of NO_2^- ions relative to negatively charged NO_3^- and IO_3^- accesses the surfaces of TA/11-MU–Au NDs more easily through the electrostatic attraction. Many studies have demonstrated that Hg^{2+}, Cu^{2+}, and H_2O_2 could cause the PL quenching of Au NCs or Au NDs.[2,3,24] However, the Hg^{2+}, Cu^{2+}, and H_2O_2 did not cause significant PL quenching of the TA/11-MU–Au ND probe (Fig. 2a). We determined NO_2^- ions using the unpurified TA/11-MU–Au ND probe in an acidic medium (10 mM sodium phosphate solution, pH 3.0). In the presence of free 11-MU in unpurified TA/11-MU–Au ND solution, Hg^{2+} and Cu^{2+} induced quenching of Au NDs was minimized, owing to the formation of the complexes of 11-MU with Hg^{2+} and Cu^{2+} ions ($K_f \sim 10^{30}$ to 10^{45} M) in the bulk solution. Although H_2O_2 is a powerful oxidizer ($H_2O_2 + 2H^+ + 2e^- \rightarrow 2H_2O$; $E^0 = 1.78$ V) in acidic medium, the intermediate (NO^+) of NO_2^- ions relative to H_2O_2 more easily accesses the surfaces of TA/11-MU–Au NDs through electrostatic attraction (Fig 2a and S8†).

Fig. 2b displays the PL response of the TA/11-MU–Au ND (5.0 nM) probe toward NO_2^- ions (0–5.0 μM) in 10 mM sodium phosphate solution (pH 3.0). This probe exhibited a linear response ($r = 0.95$) of its relative PL intensity [$(I_{PL}^0 - I_{PL})/I_{PL}$] at 520 nm with respect to the concentration of NO_2^- ions over the range 0.1–1.5 μM (inset). I_{PL}^0 and I_{PL} represent PL intensities of

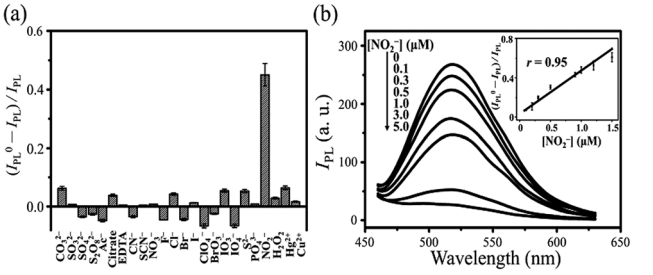

Fig. 2 Relative PL intensity [$(I_{PL}^0 - I_{PL})/I_{PL}$] of TA/11-MU–Au NDs (5.0 nM) at 520 nm in sodium phosphate solution (10 mM, pH 3.0) (a) upon the addition of 1.0 μM of NO_2^- ions or 10 μM of other anions, heavy metal ions (Hg^{2+} and Cu^{2+}) and H_2O_2 and (b) in the presence of NO_2^- ions (0–5.0 μM). Error bars represent standard deviations from three repeated experiments. Other conditions are as described in Fig. 1.

Published on 05 August 2014. Downloaded by Michigan State University on 23/01/2016 07:14:54.

the TA/11-MU–Au ND probe in the absence and presence of NO_2^- ions, respectively. At a signal-to-noise (*S*/*N*) ratio of 3, the limit of detection (LOD) for NO_2^- ions was 40 nM, which is considerably lower than the maximum level of NO_2^- ions in drinking water (approximately 21.7 μM) permitted by the U.S. Environmental Protection Agency (EPA).[25] This LOD is comparable with or better than those obtained using other nanomaterial-based sensors for NO_2^- ions.[21,26] The good selectivity and sensitivity for detecting NO_2^- ions suggests a great potential of TA/11-MU–Au NDs in analyzing the presence of NO_2^- ions in environmental samples.

To validate the practicality of our proposed sensing strategy for analysis of NO_2^- ions in drinking water and natural water samples, the TA/11-MU–Au ND probe was employed to determine concentrations of NO_2^- ions (0–1.2 μM) in samples of tap water, lake water, and seawater spiked with NO_2^-. For these three water samples, similar LODs (~50 nM) for NO_2^- ions were obtained, showing minimum matrix effects (Fig. S9, ESI†). The TA/11-MU–Au ND probe provided recoveries of NO_2^- ions at the concentration of 0.5 μM, which were 98.1%, 102.2%, and 108.4% in the tap water, lake water, and seawater samples, respectively. The recovery was highest in the seawater sample because of interference from the high concentration of salt. The presence of NO_2^- ions was not detected in water samples that were not spiked. Therefore, we believe that concentrations of NO_2^- ions in our collected water samples were below 50 nM.

In summary, a simple and convenient platform was developed for preparing photoluminescent AL/11-MU–Au NDs *via* nonspecific hydrophobic interactions of ALs and 11-MU molecules on Au ND surfaces. We demonstrated that charges, chain lengths, and functional groups of ALs (DA, DDA, TA, DTAB, MTAB, and HTAB) had strong effects on the optical properties of the Au NDs. The MTAB/11-MU–Au NDs possess the highest PL QY of 37% (at 630 nm). Among three tested FAs, TA allowed the preparation of TA/11-MU–Au NDs with the strongest PL and highest dispersibility. The TA/11-MU–Au NDs were employed to detect NO_2^- ions, based on analyte-induced PL quenching. Under acidic conditions, the TA/11-MU–Au NDs provided high sensitivity (LOD: 40 nM) and selectivity (>100-fold against other anions), allowing the detection of NO_2^- ions in tap and natural water samples. The one-pot synthesis strategy with hydrophobic interactions developed in this study opens a new approach for the synthesis of various functional Au ND probes.

Acknowledgements

This study was supported by the Ministry of Science and Technology of Taiwan under contract NSC 101-2113-M-002-002-MY3.

Notes and references

1 (*a*) R. Jin, *Nanoscale*, 2010, **2**, 343–362; (*b*) L. Shang, S. Dong and G. U. Nienhaus, *Nano Today*, 2011, **6**, 401–418; (*c*) Y.-C. Shiang, C.-C. Huang, W.-Y. Chen, P.-C. Chen and H.-T. Chang, *J. Mater. Chem.*, 2012, **22**, 12972–12982; (*d*) P. L. Xavier, K. Chaudhari, A. Baksi and T. Pradeep, *Nano Rev.*, 2012, **3**, 14767–14783; (*e*) Y. Lu and W. Chen, *Chem. Soc. Rev.*, 2012, **41**, 3594–3623; (*f*) X. Yuan, Z. Luo, Y. Yu, Q. Yao and J. Xie, *Chem.–Asian J.*, 2013, **8**, 858–871.

2 (*a*) L.-Y. Chen, C.-M. Ou, W.-Y. Chen, C.-C. Huang and H.-T. Chang, *ACS Appl. Mater. Interfaces*, 2013, **5**, 4383–4388; (*b*) H.-Y. Chang, H.-T. Chang, Y.-L. Hung, T.-M. Hsiung, Y.-W. Lin and C.-C. Huang, *RSC Adv.*, 2013, **3**, 4588–4597.

3 C.-C. Huang, Z. Yang, K.-H. Lee and H.-T. Chang, *Angew. Chem., Int. Ed.*, 2007, **46**, 6824–6828.

4 (*a*) R. Jin, Y. Zhu and H. Qian, *Chem.–Eur. J.*, 2011, **17**, 6584–6593; (*b*) J. Zheng, C. Zhou, M. Yu and J. Liu, *Nanoscale*, 2012, **4**, 4073–4083.

5 (*a*) A. Barbieri, G. Accorsi and N. Armaroli, *Chem. Commun.*, 2008, 2185–2193; (*b*) E. R. T. Tiekink and J.-G. Kang, *Coord. Chem. Rev.*, 2009, **253**, 1627–1648; (*c*) C.-C. Huang, Y.-L. Hung, Y.-C. Shiang, T.-Y. Lin, Y.-S. Lin, C.-T. Chen and H.-T. Chang, *Chem.–Asian J.*, 2010, **5**, 334–341.

6 (*a*) A. Vogler and H. Kunkely, *Coord. Chem. Rev.*, 2001, **219–221**, 489–507; (*b*) N. L. Coker, J. A. K. Bauer and R. C. Elder, *J. Am. Chem. Soc.*, 2004, **126**, 12–13; (*c*) Y. Negishi, K. Nobusada and T. Tsukuda, *J. Am. Chem. Soc.*, 2005, **127**, 5261–5270.

7 V. W.-W. Yam and E. C.-C. Cheng, *Chem. Soc. Rev.*, 2008, **37**, 1806–1813.

8 (*a*) Z. Wu and R. Jin, *Nano Lett.*, 2010, **10**, 2568–2573; (*b*) Y. Negishi, W. Kurashige, Y. Niihori and K. Nobusada, *Phys. Chem. Chem. Phys.*, 2013, **15**, 18736–18751.

9 W.-Y. Chen, L.-Y. Chen, C.-M. Ou, C.-C. Huang, S.-C. Wei and H.-T. Chang, *Anal. Chem.*, 2013, **85**, 8834–8840.

10 Y. Zhu, H. Qian and R. Jin, *J. Mater. Chem.*, 2011, **21**, 6793–6799.

11 L. Shang and G. U. Nienhaus, *Biophys. Rev.*, 2012, **4**, 313–322.

12 (*a*) C. S. Bruning-Fann and J. B. Kaneene, *Vet. Hum. Toxicol.*, 1993, **35**, 521–538; (*b*) J. A. Camargo and Á. Alonso, *Environ. Int.*, 2006, **32**, 831–849; (*c*) A. Cockburn, G. Brambilla, M.-L. Fernández, D. Arcella, L. R. Bordajandi, B. Cottrill, C. Van Peteghem and J.-L. Dorne, *Toxicol. Appl. Pharmacol.*, 2013, **270**, 209–217.

13 D. G. Duff and A. Baiker, *Langmuir*, 1993, **9**, 2301–2309.

14 (*a*) S.-H. Cho, J.-U. Kim, K.-H. Kim and J.-C. Lee, *Chem. Mater.*, 2007, **19**, 6297–6303; (*b*) B. Dong, C. Li, G. Chen, Y. Zhang, Y. Zhang, M. Deng and Q. Wang, *Chem. Mater.*, 2013, **25**, 2503–2509.

15 (*a*) X. Wen, P. Yu, Y.-R. Toh and J. Tang, *J. Phys. Chem. C*, 2012, **116**, 11830–11836; (*b*) X. Wen, P. Yu, Y.-R. Toh, A.-C. Hsu, Y.-C. Lee and J. Tang, *J. Phys. Chem. C*, 2012, **116**, 19032–19038.

16 P. Yu, X. Wen, Y.-R. Toh, Y.-C. Lee and J. Tang, *RSC Adv.*, 2013, **3**, 19609–19616.

17 (*a*) Y.-C. Jao, M.-K. Chen and S.-Y. Lin, *Chem. Commun.*, 2010, **46**, 2626–2628; (*b*) D.-E. Jiang and M. Walter, *Nanoscale*, 2012, **4**, 4234–4239.

18 Z. Luo, X. Yuan, Y. Yu, Q. Zhang, D. T. Leong, J. Y. Lee and J. Xie, *J. Am. Chem. Soc.*, 2012, **134**, 16662–16670.

19 C. Zhou, C. Sun, M. X. Yu, Y. P. Qin, J. G. Wang, M. Kim and J. Zheng, *J. Phys. Chem. C*, 2010, **114**, 7727–7732.

 This journal is © The Royal Society of Chemistry 2014

Published on 05 August 2014. Downloaded by Michigan State University on 23/01/2016 07:14:54.

20 X. Le Guével, V. Trouillet, C. Spies, K. Li, T. Laaksonen, D. Auerbach, G. Jung and M. Schneider, *Nanoscale*, 2012, **4**, 7624–7631.

21 (*a*) H. Liu, G. Yang, E. S. Abdel-Halim and J.-J. Zhu, *Talanta*, 2013, **104**, 135–139; (*b*) J. Zhang, C. Chen, X. Xu, X. Wang and X. Yang, *Chem. Commun.*, 2013, **49**, 2691–2693; (*c*) B. Unnikrishnan, S.-C. Wei, W.-J. Chiu, J. Cang, P.-H. Hsu and C.-C. Huang, *Analyst*, 2014, **139**, 2221–2228.

22 S. Ozawa, E. Sakamoto, T. Ichikawa, Y. Watanabe and I. Morishima, *Inorg. Chem.*, 1995, **34**, 6362–6370.

23 Y. Wang, E. Laborda and R. G. Compton, *J. Electroanal. Chem.*, 2012, **670**, 56–61.

24 (*a*) J. Xie, Y. Zheng and J. Y. Ying, *Chem. Commun.*, 2010, **46**, 961–963; (*b*) D. Cao, J. Fan, J. Qiu, Y. Tu and J. Yan, *Biosens. Bioelectron.*, 2013, **42**, 47–50.

25 World Health Organization, *Guidelines for Drinking Water Quality: incorporating 1st and 2nd addenda, Vol. 1, Recommendations–3rd*, WHO, Geneva, Switzerland, 60th edn, 2008.

26 (*a*) W. L. Daniel, M. S. Han, J.-S. Lee and C. A. Mirkin, *J. Am. Chem. Soc.*, 2009, **131**, 6362–6363; (*b*) Z. Lin, W. Xue, H. Chen and J.-M. Lin, *Anal. Chem.*, 2011, **83**, 8245–8251; (*c*) L. Wang, B. Li, L. Zhang, L. Zhang and H. Zhao, *Sens. Actuators, B*, 2012, **171–172**, 946–953; (*d*) S. Dong, W. Guan and C. Lu, *Sens. Actuators, B*, 2013, **188**, 597–602.